Available online at www.sciencedirect.com
ScienceDirect
Journal of Magnetism and Magnetic Materials 313 (2007) 187–191
Journal of magnetism and magnetic materials
www.elsevier.com/locate/jmmm

Tunable negative index metamaterial using yttrium iron garnet

Yongxue He[a,b,*], Peng He[a,b], Soack Dae Yoon[a,b], P.V. Parimi[c], F.J. Rachford[d], V.G. Harris[a,b], C. Vittoria[a,b]

[a]*Center for Microwave Magnetic Materials and Integrated Circuits, Northeastern University, Boston, MA 02115, USA*
[b]*Department of Electrical and Computer Engineering, Northeastern University, Boston, MA 02115, USA*
[c]*Physics Department, Northeastern University, 360 Huntington Avenue, Boston, MA 02115, USA*
[d]*Code 6362, Naval Research Laboratory, 4555 Overlook Ave SW, Washington, DC 20375, USA*

Received 11 December 2006
Available online 14 February 2007

Abstract

A magnetic field tunable, broadband, low-loss, negative refractive index metamaterial is fabricated using yttrium iron garnet (YIG) and a periodic array of copper wires. The tunability is demonstrated from 18 to 23 GHz under an applied magnetic field with a figure of merit of 4.2 GHz/kOe. The tuning bandwidth is measured to be 5 GHz compared to 0.9 GHz for fixed field. We measure a minimum insertion loss of 4 dB (or 5.7 dB/cm) at 22.3 GHz. The measured negative refractive index bandwidth is 0.9 GHz compared to 0.5 GHz calculated by the transfer function matrix theory and 1 GHz calculated by finite element simulation.
© 2007 Published by Elsevier B.V.

PACS: 42.25.Bs; 41.20.Jb; 73.20.Mf

Keywords: Negative index media; Ferrite; Garnet; Metamaterial; Tunable

There has been considerable interest in the development of metamaterial composites that possess negative dielectric (ε) and permeability (μ) constants coincident in frequency giving rise to a negative index of refraction (n) [1]. These constructs are generally referred to as negative index metamaterials or NIMs. Much of the fascination in NIMs arises from their unusual electromagnetic properties such as backward wave propagation and subwavelength resolution imaging [2] that allow for several novel applications such as super lenses [3], leaky wave antennas [4], and miniature delay lines. Notable NIMs are resonant metamaterials [5,6], photonic crystals [7–10], and planar periodic arrays of passive lumped circuit elements [11]. These NIMs are limited by inherent narrow bandwidth and are not at all tunable. In order to obtain negative n at various frequencies, one would have to change the periodicity and size of the elements. Additionally, it is difficult to scale these materials to terahertz and visible frequencies. Recently, several metamaterial and ferrite structures have been proposed [12–14].

In this paper, we present experimental results of an electronically tunable NIM using yttrium iron garnet and an array of copper wires. We also demonstrate a key feature of magnetic field tunability of the NIM in the microwave frequency region. The field tunable NIM presented here allows experimental investigation of the nonlinear properties and harmonic response of the NIMs that have until now only been investigated theoretically [15–17]. The control achieved on material parameters and tunability could pave the way for the development NIM microstrip, stripline [18], and coplanar guided wave structures.

We demonstrate a scheme by which continuous frequency tuning of the negative index is possible by using a YIG film or slab. The effect of the YIG film is to provide a tunable negative μ over a continuous range of frequencies on the high-frequency side of the ferrimagnetic resonance. Complementary negative ε is achieved using a single

*Corresponding author. Center for Microwave Magnetic Materials and Integrated Circuits, Northeastern University, Boston, MA 02115, USA.
E-mail address: flypeyton@gmail.com (Y. He).

0304-8853/$ - see front matter © 2007 Published by Elsevier B.V.
doi:10.1016/j.jmmm.2006.12.031

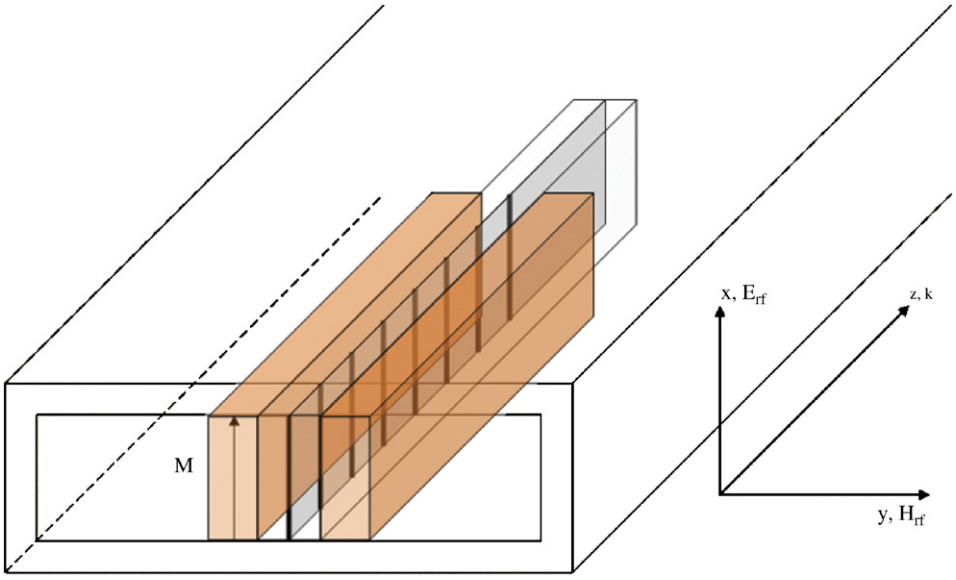

Fig. 1. Schematic diagram of the experimental setup showing the NIM composite inserted in a K-band waveguide (inside dimensions: 1.07 cm by 0.43 cm). The composite structure consisted of eight copper wires spaced 1 mm apart and multilayered YIG films with a total thickness of 400 μm. The shaded regions are YIG films whereas the black lines represented copper wires. Notice that the ferrite is separated from the wires by a nonmagnetic dielectric material.

periodic array of copper wires. Fig. 1 shows a schematic diagram of this tunable NIM in a K-band waveguide. The composite structure consists of eight copper wires spaced 1 mm apart and a multilayered YIG film with a total thickness of 400 μm. YIG films were deposited by liquid phase epitaxy on both sides of a GGG (gadolinium gallium garnet) substrate. The thickness of the GGG substrate was 500 μm. The condition for FMR was obtained by applying the external magnetic field, H, along x-axis (see Fig. 1).

As can be seen in Fig. 1, an air gap is maintained between the periodic array of copper wires and the YIG slab in order to reduce the coupling between the wires and the ferrite. In the frequency regime where μ is negative the close proximity of the ferrite to the wires implies a reduction in net current flow in the wires and, therefore, toward positive ε [12]. The separation also reduces the effective dielectric loss induced by the interaction of the wire self field with Im(μ). In the copper wires there are two sources of conduction: (1) the microwave electric field in a waveguide produces a current in the wire, and (2) any extraneous microwave magnetic field due to the ferrite excited in a precessional motion induces an electric field along the wires. Clearly, proximity of the ferrite plays an important role. At frequencies where μ is negative, the induced microwave magnetic field is opposite to the field excited in a TE_{10} mode of propagation in a waveguide. Hence, the induced current by mechanism (2) is opposite to the current resulting from the electric field in a waveguide, i.e., mechanism (1).

In fabricating the NIM, the copper wires were prepared by traditional lithographic techniques resulting in an array of eight wires, 25 μm thick and 100 μm in width, spaced 1 mm apart. The single crystal YIG was cut to form two 7 mm × 4 mm pieces. The composite was placed in the center of a K-band (18–26 GHz) waveguide as depicted in Fig. 1. S-parameters were measured using an HP 8510 network analyzer (45 MHz–40 GHz). An electromagnet was used to generate the external magnetic field.

The magnitude and phase of S_{21} (transmission coefficient) as measured using the network analyzer at K-band with a bias field of 6.9 kOe, are shown in Fig. 2. In order to improve the impedance mismatch at the input of the device, we used a pair of E–H tuners connected before and after the waveguide containing the NIM composite. The pass band where the loss is smaller than 6 dB is 0.9 GHz centered at 22.3 GHz.

The material parameters n_{eff}, ε_{eff} and μ_{eff} can be determined from the measured scattering parameters by the following expressions [19]:

$$\varepsilon_{\text{eff}} = \frac{n_{\text{eff}}}{Z_{\text{eff}}}, \tag{1}$$

$$\mu_{\text{eff}} = n_{\text{eff}} \cdot Z_{\text{eff}}, \tag{2}$$

$$n_{\text{eff}} = \pm \frac{c}{2\pi \cdot f \cdot L} \cos^{-1}\left(\frac{1 - S_{11}^2 + S_{21}^2}{2S_{21}}\right), \tag{3}$$

$$Z_{\text{eff}} = \pm \sqrt{\frac{(1 + S_{11})^2 - S_{21}^2}{(1 - S_{11})^2 - S_{21}^2}}. \tag{4}$$

The real and imaginary parts of index of refraction were calculated using Eq. (3) and are shown in Fig. 3. When the composite structure is sufficiently narrow that the E_{rf}, electric field, and the H_{rf}, magnetic field, are approximately uniform over the center region of the waveguide. There is no longitudinal E_{rf} and a small (or negligible) longitudinal

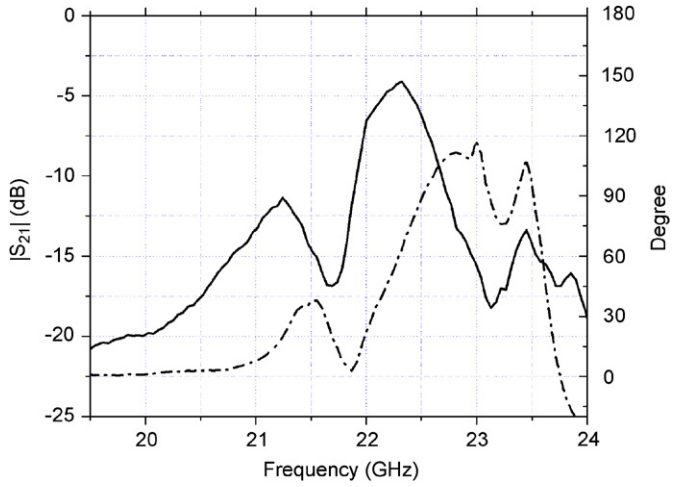

Fig. 2. Experimentally measured amplitude (solid line) and phase (dashed line) of S_{21} of the NIM inserted in the K-band waveguide.

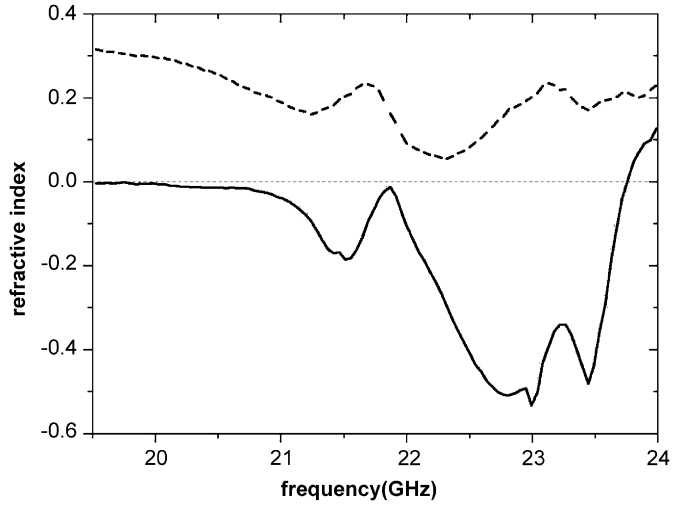

Fig. 3. Real (solid line) and imaginary (dashed line) parts of the index of refraction calculated from experimental data.

H_{rf} fields in the region. We define the refractive index as $n = n' + in''$, where $i = \sqrt{-1}$. Fig. 3 shows the plot of n_{eff}, as a function of frequency. The ambiguity in Eqs. (3) and (4) with respect to sign is eliminated by considering $n'' = \mathrm{Im}(n) > 0$ and $Z' = \mathrm{Re}(Z) > 0$. In Fig. 3, the major downward peak of n' centered at 23 GHz represents the negative refractive index region.

To demonstrate the tunability of the NIM we have carried out measurements of transmission coefficient in different external magnetic fields. Fig. 4 shows peak shift of the region of negative index with the applied field. While varying the field from 5.8 to 7.0 kOe, we observed that the magnitude of S_{21} shifted from 18 to 23 GHz. (The E–H tuners were removed for this measurement since these are narrow band devices.) The *tuning* bandwidth for which the insertion loss was varied from −10 to −4 dB was 5 GHz, (the magnetic field was varied from 5.8 to 7 kOe). The fixed field bandwidth was 0.9 GHz. The bandwidth was defined

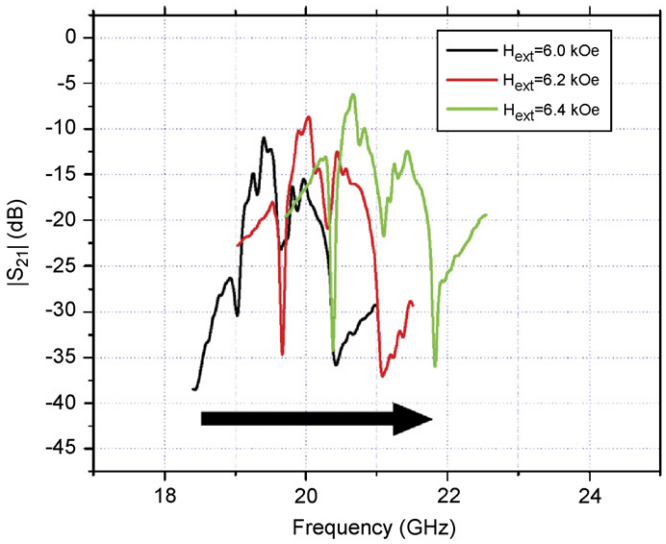

Fig. 4. Demonstration of electronic tunability of the NIM using external field. Large arrow at the bottom denotes the direction of frequency shift with increasing magnetic field.

as the frequency points when the insertion loss increases to −6 dB relative to the center frequency, 22.3 GHz. We believe that the insertion loss can be further improved with the use of E–H tuners at each magnetic field setting and refinement of the copper wire arrays. As a comparison, SRR NIMs operating at the X-band have been reported to have bandwidths $\leqslant 0.7$ GHz at a single frequency without the ability to actively tune n [20].

The experimental results presented above can be understood using the theoretical transfer function matrix (TFM) analysis. In analyzing the wave propagation in the ferrite and wire composite we assumed a TEM wave propagation within a simpler composite which has the wires and the ferrites pieces in series as shown in the inset of Fig. 5. We would expect that the TFM analysis to be reasonably accurate in predicting the frequency region where the index may be negative, since FMR condition is contained within the formulation of the TFM theory. We have also carried our finite element simulation (using Ansoft HFSS) to support the theory. In the simulation, a slab of the periodic copper wires and YIG pieces in series was set at the middle of the waveguide, where the same material and geometrical parameters were applied as in the case of TFM analysis.

We assumed that the width of the wire is sufficiently large compared to the skin depth so that propagation effects within the wire may be ignored. Hence, the wire is treated as a lumped element rather than a continuous medium [13]. We represent the wire as a lumped element having an admittance Y. The TFM [21] representing the wire is

$$[A_1] = \begin{bmatrix} 1 & 0 \\ Y & 1 \end{bmatrix}, \tag{5}$$

where

$$Y = (l/2\pi r(\sqrt{\omega\mu_0/2\sigma})(1 - i) - i\omega\mu_0 l(\ln(d/r)/2\pi))^{-1},$$

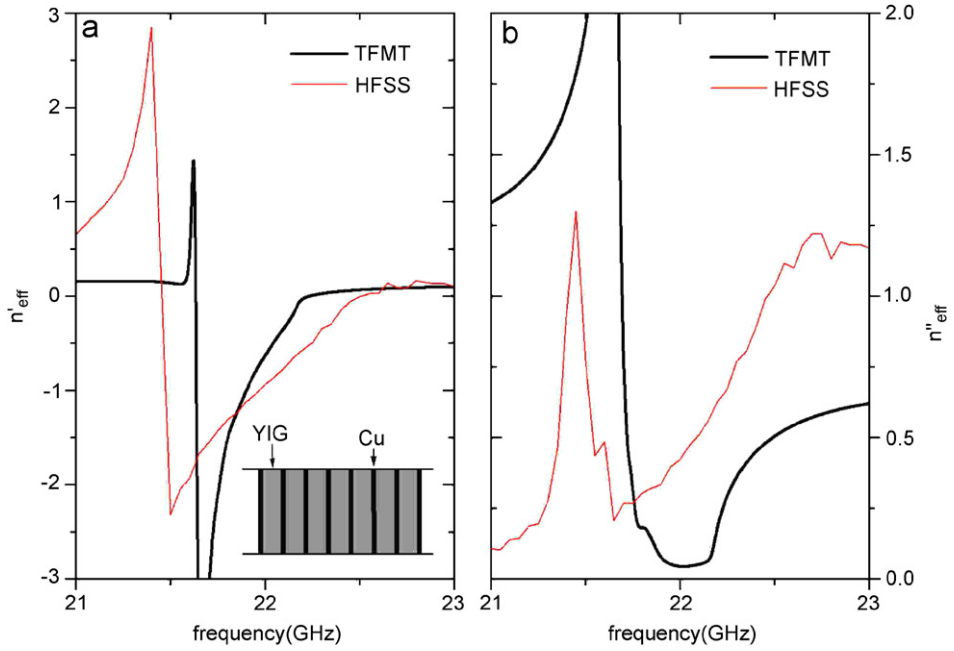

Fig. 5. Real and imaginary parts of the effective refractive index calculated from the transfer function matrix theory (black line) and simulated using finite element method (red line). The inset shows the simplified structure of copper wires and YIG films in series.

σ = conductivity, μ_0 = permeability of air, l = length of wire, r = radius of the wire, d = distance between wires and ω = angular frequency. The admittance of the wire, Y, comes from two parts, surface impedance and self-inductance. Surface impedance is related to the electromagnetic field within the wire and self-inductance is related to the electromagnetic field around wire. Since the medium between two successive wires is continuous the TFM is simply

$$[A_2] = \begin{bmatrix} \cos(kd) & -iZ\sin(kd) \\ -i\sin(kd)/Z & \cos(kd) \end{bmatrix}, \quad (6)$$

where $Z = \sqrt{\mu/\varepsilon}$, $k = \omega\sqrt{\mu\varepsilon}$, ε = dielectric constant and $\mu = (\mu_{xx}^2 + \mu_{xy}^2)/\mu_{xx}$. If the medium is not transversely uniform, average values of ε and μ should be used.

The TFM representing the composite as a whole is simply

$$[A] = \{[A_1]\cdot[A_2]\}^N = \begin{bmatrix} a_{11} & a_{12} \\ a_{21} & a_{22} \end{bmatrix}. \quad (7)$$

The fact that the resultant matrix $[A]$ is still a 2×2 matrix allows us to express its elements, a_{ij}, in terms of effective permittivity, ε_{eff}, and effective permeability, μ_{eff}. Clearly, $\varepsilon_{\text{eff}} \neq \varepsilon$ and $\mu_{\text{eff}} \neq \mu$, since ε_{eff} and μ_{eff} include the electromagnetic interaction between the wires and magneto-dielectric medium where $S_{21} = 2Z_0/(a_{12} + (a_{11} + a_{22})Z_0 + a_{21}Z_0^2)$, and $S_{11} = (a_{12} + (a_{11} - a_{22})Z_0 - a_{21}Z_0^2)/(a_{12} + (a_{11} + a_{22})Z_0 + a_{21}Z_0^2)$.

In order to test the reliability or accuracy of the TFM calculational method, we have also calculated n'_{eff} and n''_{eff} using HFSS. In Fig. 5, the solid lines are the results calculated from the S-parameters obtained from the TFM calculation whereas the dash lines are the results calculated from the simulated S-parameters using HFSS. Both results make use of Eq. (3). In Fig. 5, n'_{eff} is negative for both calculational methods. n'_{eff}, calculated by HFSS, shows a wider bandwidth (~1 GHz), whereas TFM theory predicts a narrower bandwidth (~0.5 GHz). The large values in n'_{eff} for the TFM method is a reflection of overestimating the ferrite volume, noticing that the TFM analysis is one-dimensional so that the thickness of the YIG films is not considered. While in the HFSS simulation, we set the thickness of YIG films as 0.4 mm.

In this calculation, we have used the following parameters: $\sigma = 5.8\times 10^7$ siemens/m, $l = 0.43$ cm, $r = 12.5\,\mu$m, $d = 1$ mm, $4\pi M_s = 1750$ G and $H_{\text{ext}} = 6.9$ kOe. The obvious conclusion is that the electromagnetic interaction and the dimensions of the waveguide affect the electrical parameters of the material constituents that make up the NIM. For example, if we calculate ε using the finite element method software (i.e. Ansoft HFSS$^{\text{TM}}$) allowing for three-dimensional variations and the TE_{10} mode of propagation in the waveguide, we find that $\varepsilon \approx 1 - (\omega_p/\omega)^2$, where $\omega_p/2\pi = 27.2$ GHz. The above result compares well with our one-dimensional analysis which gives $\omega_p/2\pi = 28$ GHz. The behavior of ε as a function of frequency, as calculated from the one-dimensional analysis, is very similar to that calculated using the HFSS$^{\text{TM}}$ software. In essence, ε as calculated here, contains the correct "picture" of a negative permittivity which is important in our search for a negative index of refraction in waveguided structures.

It is well known that the FMR resonance can be tuned by the application of an external magnetic field, H. Accordingly, the range of frequencies by which μ is

negative is given by

$$\Delta f = f_0 - f_r \approx \frac{\gamma}{2\pi}(2\pi M_s), \tag{8}$$

where $f_r = \gamma/2\pi\sqrt{H(H+4\pi M_s)}$, $\gamma/2\pi = 2.8\,\mathrm{GHz/kOe}$, $4\pi M_s = 1750\,\mathrm{G}$, $f_r = \mathrm{FMR}$ frequency and $f_0 \approx f_r + \gamma/2\pi(2\pi M_s)$. The subscript "0" is to denote the anti-resonance frequency at which $\mu = 0$. The object of tuning is to vary H such that f_r is varied according to Eq. (8), and, therefore, the onset of the frequency range at which μ is negative, can be shifted with H. However, the range of frequencies for which μ is negative is approximately constant and is given as $\gamma/2\pi(2\pi M_s)$. The factor of $2\pi M_s$ is a result of applying H in the film plane. If H is applied perpendicular to the film plane, Δf would scale as $4\pi M_s$. Clearly, if we are to realize a negative index we require both μ and ε to be negative. This means that irrespective of H, f_0 should not exceed f_p, the electric plasma frequency of the wires below which ε is negative. If we choose $f_0 = f_p$, the maximum applied field used for tuning is $H_{\max} \approx \omega_p/\gamma - 2\pi M_s$. Note that it may not be possible to tune f_p, if only conductive wires are used. However, since the region of negative ε is broadband this does not pose a significant limitation to practical devices.

In summary, we have demonstrated a broadband, low-loss, and tunable negative index metamaterial employing ferrite materials and copper wires. The tunability was demonstrated from 18 to 23 GHz under an applied magnetic field with a figure of merit of 4.2 GHz/kOe. The *tuning bandwidth* was measured to be 5 GHz compared to 0.9 GHz for fixed field. Conventional SRR NIMs have bandwidths at X-band of $\leqslant$0.7 GHz (or 7.4 dB/cm) [19]. We have measured a minimum transmission loss of 4 dB (or 5.7 dB/cm) at 22.3 GHz. Theoretical analysis using transfer matrix method (TFM) and finite element method simulations match with the experimental results reasonably well. In future, we plan to use self-biased ferrites [22], which require smaller applied magnetic fields and transfer the tunable NIM technology to integrated microwave devices, microstrip, stripline, or coplanar guided wave structures, Furthermore, the utilization of semiconductor films instead of copper wires should provide the opportunity to tune ε by injection of carriers via light of field effect transistors.

This work was sponsored by a Grant from the Defense Advanced Research Program Agency.

References

[1] V.G. Veselago, Sov. Phys. Usp. 10 (1968) 509.
[2] N. Fang, H. Lee, C. Sun, X. Zhang, Science 308 (2005) 534.
[3] J.B. Pendry, Phys. Rev. Lett. 85 (2000) 3966.
[4] S. Lim, C. Caloz, T. Itoh, IEEE Microwave Wireless Components Lett. 14 (2004) 277.
[5] D.R. Smith, W.J. Padilla, D.C. Vier, S.C. Nemat-Nasser, S. Schultz, Phys. Rev. Lett. 84 (2000) 4184.
[6] R.A. Shelby, D.R. Smith, S. Schultz, Science 292 (2001) 77.
[7] S. Foteinopoulou, E.N. Economou, C.M. Soukoulis, Phys. Rev. Lett. 90 (2003) 107402.
[8] M. Notomi, Phys. Rev. B 62 (2000) 10696.
[9] P.V. Parimi, W.T. Lu, P. Vodo, J. Sokoloff, J.S. Derov, S. Sridhar, Phys. Rev. Lett. 92 (2004) 127401.
[10] C. Luo, S.G. Johnson, J.D. Joannopoulos, Phys. Rev. B 65 (2002) 201104.
[11] C. Caloz, T. Itoh, IEEE Trans. Antennas Propag. 52 (2004) 1159.
[12] G. Dewar, J. Appl. Phys. 97 (2005) 10Q101.
[13] R.X. Wu, J. Appl. Phys. 97 (2005) 076105.
[14] A. Pimenov, A. Loidl, P. Przyslupski, B. Dabrowski, Phys. Rev. Lett. 95 (2005) 247009.
[15] A.B. Kozyrev, H. Kim, A. Karbassi, D.W. van der Weide, Appl. Phys. Lett. 87 (2005) 121109.
[16] I.V. Shadrivov, A.A. Zharov, N.A. Zharova, Y.S. Kivshar, Radio Sci. 40 (2005) RS3S90.
[17] N. Garcia, E.V. Ponizovskaia, Phys. Rev. E 71 (2005) 04661.
[18] C.M. Krowne, Phys. Rev. Lett. 92 (2004) 053901.
[19] D.R. Smith, S. Schultz, P. Markos, C.M. Soukoulis, Phys. Rev. B 65 (2002) 195104.
[20] A.F. Starr, P.M. Rye, D.R. Smith, S. Nemat-Nasser, Phys. Rev. B 70 (2004) 113102.
[21] C. Vittoria, Elements of Microwave Networks, World Scientific, Singapore, 1998.
[22] Y. Chen, T. Sakai, T. Chen, S. Yoon, A. Geiler, C. Vittoria, V. Harris, Appl. Phys. Lett. 88 (2006) 062516.